1

Folding and Three-Dimensional NMR Structure of the Recombinant Cellular Prion Protein from the Mouse

Rudi Glockshuber, Simone Hornemann, Roland Riek, Martin Billeter, Gerhard Wider, Susanne Liemann, Ralph Zahn and Kurt Wüthrich

Abstract

The NMR structure of the recombinant mouse prion protein in the cellular form (mPrP^{C}) contains a flexible disordered N-terminal segment of residues 23–125 and a novel globular fold with three α-helices and a small β-sheet formed by the C-terminal residues 126–231. The presumed infectious agent of transmissible spongiform encephalopathies (TSEs), PrP^{Sc}, differs from PrP^{C} at least with respect to the conformation of the segment 90–125, which is resistant to proteolysis in PrP^{Sc} but disordered and accessible in PrP^{C}. At acidic pH the fragment mPrP(121–231) can adopt an alternative conformation with increased β-sheet content, which may relate to the presumed conversion of PrP^{C} to PrP^{Sc} in acidic endosomes. Biochemical experiments and analysis of the locations in the structure of mPrP^{C} of the point mutation sites linked with familial human TSEs indicate that destabilization of PrP^{C} cannot be a general mechanism favoring formation of PrP^{Sc} in inherited TSEs. Amino acid substitutions among the highly conserved mammalian prion proteins are clustered in four distinct regions in the three-dimensional structure of mPrP(121–231). Three of these regions represent potential surface recognition sites that may be involved in intermolecular interactions related to the species barrier for infectious transmission of TSEs.

Introduction

The "protein-only" hypothesis (1–3) proposes that the infectious agent of transmissible spongiform encephalopathies (TSEs), such as Creutzfeldt-Jakob disease (CJD) in humans, scrapie in sheep and bovine spongiform encephalopathy (BSE) in cattle, consists of an abnormal, oligomeric form, PrP^{Sc}, of the host-encoded, monomeric cellular prion protein, PrP^{C}. The three principal assumptions underlying this hypothesis are that PrP^{C} and PrP^{Sc} have identical covalent structures, that PrP^{C} and PrP^{Sc} differ exclusively in their three-dimensional structures, and that PrP^{Sc} could propagate *in vivo* by imposing its fold on PrP^{C}. This hypothesis of the replication of the scrapie agent in the apparent absence of infectious nucleic acids is based on analytical and genetic data (4–6). Nevertheless, the "protein-only" hypothesis appears to contradict one of the central dogmas of protein chemistry, namely that a unique three-dimensional structure of a protein is encoded by its amino acid sequence (7). Indeed, infrared spectroscopy and circular dichroism data suggest that PrP^{C} and PrP^{Sc} monomers have different three-dimensional structures. While PrP^{C} mostly contains α-helical secondary structures, PrP^{Sc} shows a high content of β-sheets (8, 9). It is thus obvious that knowledge of the three-dimensional structures of PrP^{C} and PrP^{Sc} is of crucial importance for understanding the molecular events during the presumed propagation of the infectious PrPSc. As the only form of PrP^{Sc} that has so far been characterized is insoluble and seems inaccessible for structure determination at the atomic level, the structure of the soluble PrP^{C} monomer is of central interest. Lack of sufficient amounts of PrP^{C} for biophysical studies appears to be the main reason why only scarce data on folding and three-dimensional structure of PrP^{C} was available until recently. The topic of this chapter is the establishment of efficient production of recombinant PrP^{C}, the determination of its three-dimensional structure in solution by nuclear magnetic resonance (NMR) spectroscopy, and the characterization of PrP^{C} with respect to folding and possible conformational polymorphism.

Production, folding, stability and pH-dependent conformational changes of the recombinant cellular prion protein from the mouse, *m*PrP(23–231), and its C-terminal domain, *m*PrP(121–231)

Expression of the recombinant murine prion protein in *Escherichia coli* and identification of its C-terminal domain

The primary structure of mammalian prion proteins is highly conserved between different species, and pairs of sequences are generally more than 90% identical (10, 11). As sequence identity larger than 25% with a protein of known structure is

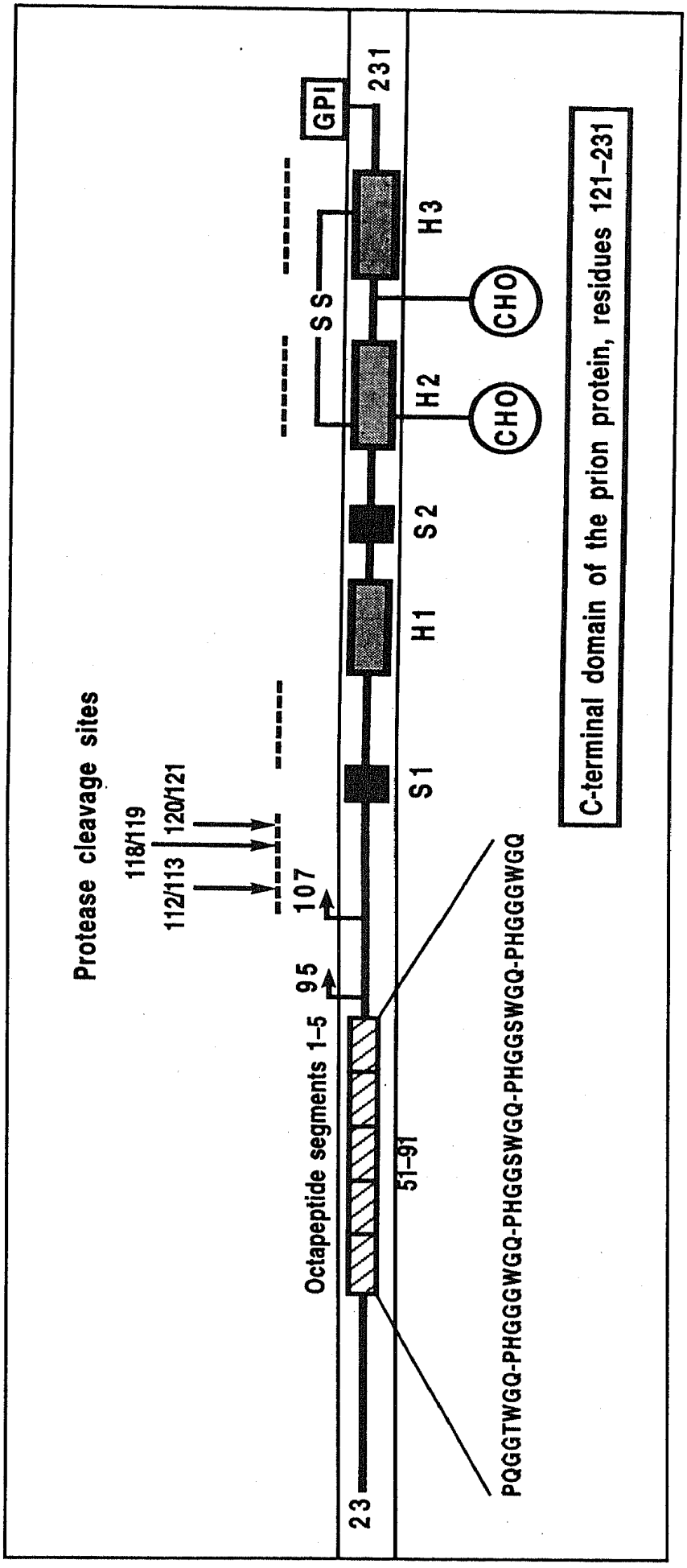

Figure 1. Schematic presentation of the primary structure and the posttranslational modifications of mammalian PrP (amino acids 23-231) and identification of the globular C-terminal domain of PrP^C. Based on the predicition that residues 109-231 of PrP^C form a four-helix-bundle protein (the positions of the four predicted helices are marked by dashed lines above the sequence) (16), the fragments 95-231 and 107-231 (bent arrows) were secreted to the periplasm of *E. coli*. Edman sequencing of the recombinant proteins revealed proteolytic degradation at the N-termini with cleavage after residues 112, 118 and 120. The segment 121-231 was stable against further proteolytic cleavage *in vivo*. The determination of the three-dimensional structure of *m*PrP(121-231) (20) revealed that the C-terminal domain of *m*PrP^C consists of three α-helices (H1, H2, H3) and a two-stranded antiparallel β-sheet (S1, S2). The five octapeptide repeats forming the segment 51-91 are indicated. Posttranslational modifications of natural PrP^C are the two glycosylations at Asn181 and Asn197, the single disulfide bridge between Cys179 and Cys214, and the GPI anchor at the C-terminal Ser231.

generally sufficient for a prediction of the overall fold of a new protein, all mammalian prion proteins are likely to possess similar three-dimensional structures. Therefore, the presently described biophysical and structural studies on the cellular prion protein from the mouse should provide a useful basis for structure–function correlations also in other mammalian prion proteins.

The development of bacterial expression systems that allowed the production of milligram amounts of pure, soluble PrP^C opened the avenue for biophysical and structural studies on PrP^C. The procedures used for PrP^C production were based on consideration of the following biochemical properties. Murine PrP^C is a monomeric cell surface glycoprotein of 208 amino acids (amino acid numbering according to the human and hamster prion protein (10)) which is anchored to the cell surface via a glycosyl-phosphatidyl-inositol (GPI) moiety at its C-terminal residue (Ser 231) (12). It contains two glycosylation sites at Asn181 and Asn197, and a single disulfide bridge between Cys179 and Cys214 (12) (cf. Fig. 1). The presence of the single disulfide bridge is essential for the stability of PrP^C and the integrity of its three-dimensional structure (13), and its formation is of critical importance for obtaining large quantities of recombinant PrP^C from *Escherichia coli*. Since the formation of a disulfide bridge is an oxidation process that does not occur in the reducing environment of the cytoplasm, the polypeptide corresponding to mature murine PrP^C (residues 23–231) accumulates in insoluble inclusion bodies upon expression in the cytoplasm of *E. coli*. Therefore, PrP^C had to be refolded *in vitro* by solubilisation of the inclusion bodies in concentrated urea solutions, oxidation of the single disulfide bridge and removal of the urea. Correctly folded, recombinant PrP^C was then obtained by purification with conventional chromatographic techniques (14).

Alternatively, recombinant mammalian PrP(23–231) can be produced by "high affinity-column refolding" (15). The protein is expressed in *E. coli* with a N-terminal histidine tail fusion into cytoplasmic inclusion bodies, and refolded and oxidized while immobilized on a Ni^{2+}–NTA agarose resin (52). This procedure facilitates the preparation of prion protein by preventing protein aggregation and intermolecular disulfide bond formation. After elution of the oxidized protein from the resin the histidine tail can be specifically cleaved off by thrombin without any degradation of PrP(23–231). Using this method, recombinant human and bovine full-length PrP and fragments thereof, *e.g.*, the polypeptides comprising residues 81–231, 90–231 and 121–231 have successfully been produced (15). In all preparations of prion protein fragments that are longer than PrP(121–231), extreme care had to be used throughout isolation and purification to prevent proteolytic degradation. The proteins thus obtained are stable for weeks at room temperature at high concentration and are thus suitable for detailed structural studies by NMR.

A different expression method for disulfide-bonded proteins in bacteria is their secretion into the oxidizing environment of the periplasmic space, where the disulfide bonds can form *in vivo*. However, attempts to produce correctly folded, soluble *m*PrP(23–231) in the periplasm of *E. coli* proved to be unsuccessful (13, 14). In contrast, secretion of certain fragments of the mouse prion protein into the periplasm of *E. coli* yielded soluble proteins, but biochemical analysis of the periplasmically expressed segments 95–231 and 107–231 revealed that both proteins were N-terminally degraded, presumably by periplasmic *E. coli* proteases. At

the outset of our project these segments were chosen to check on the validity of theoretical model predictions for the region 109–231 of PrP^C (16). All identified cleavage sites were located within a predicted α-helix with residues 109–122 of PrP^C (17) (Fig. 1). Because proteolytic cleavage of folded proteins generally occurs at domain boundaries or within exposed loop regions rather than within regular secondary structures (18), this was a first hint that the proposed four-helix-bundle model was incorrect and that only the shorter segment 121–231 represents an intrinsically stable domain. This segment corresponding to the C-terminal 111 residues of the mouse prion protein was designated *m*PrP(121–231) (17).

Spectroscopic characterization of the recombinant full-length mouse prion protein *m*PrP(23–231) and its C-terminal domain *m*PrP(121–231)

Circular dichroism (CD) and fluorescence spectra of *m*PrP(23–231) and *m*PrP(121–231) were recorded for a first structural characterization of the recombinant proteins (14, 17). Both show very similar CD spectra in the far-UV region, with two minima at 222 nm and 208 nm that are diagnostic for high content of α-helices (Fig. 2A). The normalized signal intensity was significantly lower for *m*PrP(23–231) when compared to its C-terminal domain, which indicated absence of regular secondary structure in the N-terminal segment 23–120 (16) (Fig. 2A). A similar result was obtained for the near-UV CD-spectra of *m*PrP(23–231) and *m*PrP(121–231), which are a measure for the extent of tertiary structure formation (17) (Fig. 2B). The fluorescence spectra of the proteins (Fig. 2C) also indicated that the region 23–120 is extended and solvent-exposed, since its 7 tryptophan indoles show an emission maximum of 345 nm, which is near the value of 348 nm for free tryptophan in solution. Preliminary biophysical characterization of human and bovine PrP(23–231) suggests that these proteins have the same domain architecture as *m*PrP(23–231), with analogous unstructured N-terminal segments and structured C-terminal domains (15; R. Zahn, L.G. Francisco, A. Liu, R. Riek, G. Wider and K. Wüthrich, unpublished results).

In summary, the spectroscopic properties of recombinant *m*PrP(23–231) and *m*PrP(121–231) are in full agreement with those of PrP^C purified from eukaryotic cells (9), indicating that the three-dimensional structure of recombinant *m*PrP(23–231) is identical with that of natural PrP^C, and hence that glycosylation at Asn181 and Asn197 and fusion with the GPI-anchor at Ser 231 have at most a minor influence on the structure and folding of PrP^C. In addition, analytical gel filtration studies revealed that *m*PrP(121–231) is monomeric in solution (19), which also coincides with natural PrP^C.

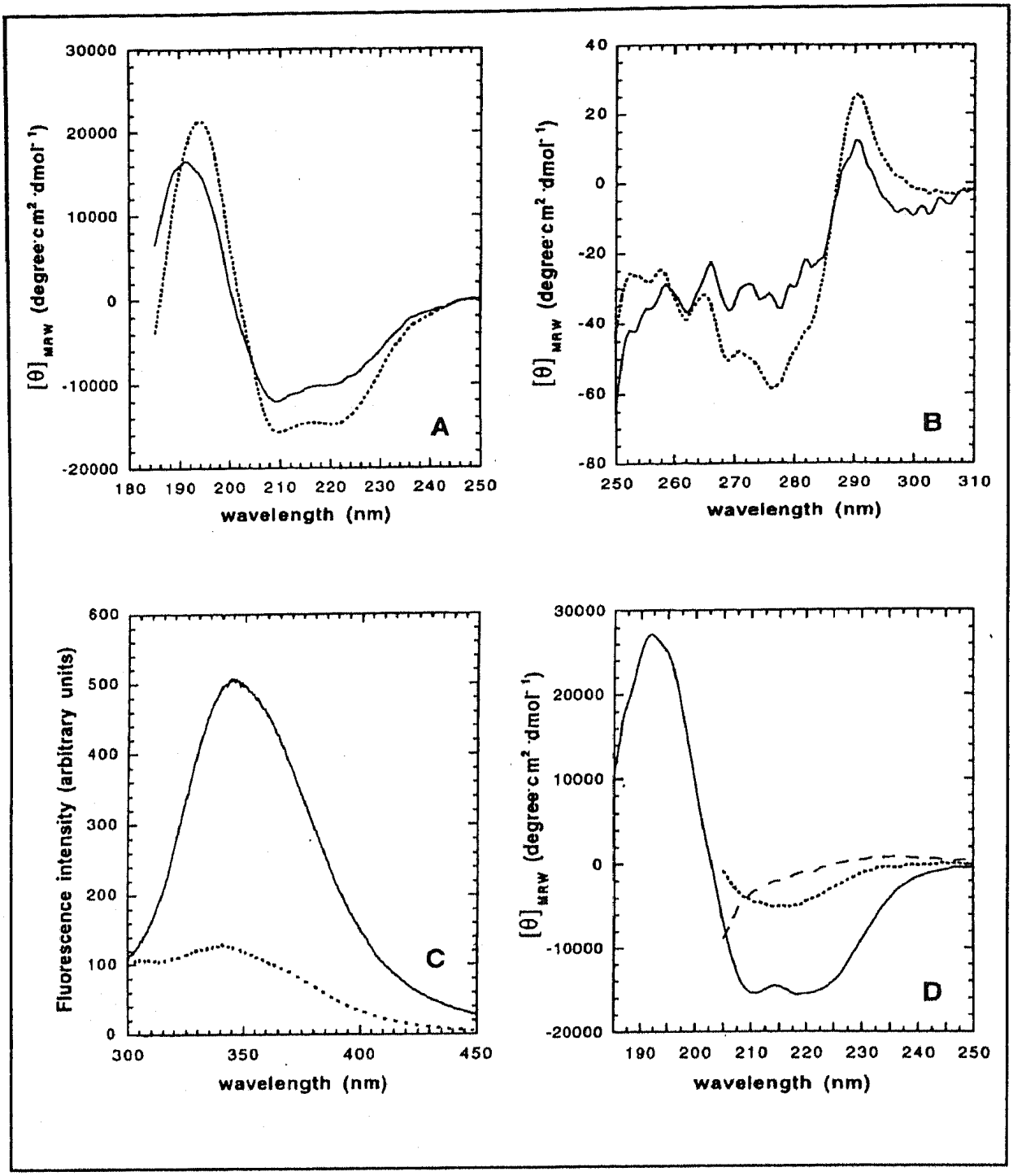

Figure 2. Comparison of spectroscopic characteristics of recombinant murine PrP^C and its C-terminal domain *m*PrP(121–231). The far-UV (A) and near-UV (B) CD spectra as well as the fluorescence spectra (C) of the full-length protein (–) and of the C-terminal domain (···) at pH 7.0 and 22°C are shown. Identical protein concentrations of 0.75 mM were used for recording the fluorescence spectra (excitation wavelength: 280 nm). (D) Spectroscopic characterization of the equilibrium unfolding intermediate of *m*PrP(121–231) induced at pH 4.0 (cf. Fig. 3). The far-UV CD spectra of native *m*PrP(121–231) at pH 4.0 (–), the unfolding intermediate of *m*PrP(121–231) at pH 4.0 and 3.5 M urea (···), and the denatured *m*PrP(121–231) (- -) are shown.

Reversibility and pH-dependence of folding and stability of *m*PrP(121–231)

Murine PrP(121–231) was found to fold cooperatively and reversibly in guanidinium chloride (GdmCl)- and urea-dependent unfolding/refolding transitions monitored at pH 7.0 by the decrease of the CD signal at 222 nm (17, 22) (Fig. 3A). Analysis of the urea-induced unfolding transition of *m*PrP(121–231) at pH 7.0 according to the two-state model of folding (23) yielded a free energy of folding of –8.6 kJ/mol (22).

Within the framework of the "protein-only" hypothesis, the reversible unfolding of *m*PrP(121–231) by GdmCl and urea has an important implication if one assumes that natural PrP^{C} with its posttranslational modifications also folds reversibly. If PrP^{C} and PrP^{Sc} indeed have identical covalent structures (12), both forms of the prion protein will yield identical unfolded molecules in the presence of high concentrations of GdmCl or urea. After reconstitution *in vitro* one therefore obtains folded PrP^{C}, independently of whether the experiments were started with PrP^{C} or PrP^{Sc}. This would explain why attempts to reconstitute infectivity after solubilization of PrP^{Sc} with high concentrations of denaturants have failed (24).

Further denaturation experiments in the presence of urea demonstrated that folding pathways and stability of *m*PrP(121–231) are pH-dependent (22). Figure 3A shows that the unfolding transitions of *m*PrP(121–231) are shifted to lower urea concentrations with decreasing pH, which demonstrates that acidic pH destabilizes the C-terminal domain of $mPrP^{C}$. In addition, the unfolding transitions of *m*PrP(121–231) at pH 4.0 and pH 4.5 are no longer one-step processes and involve at least three molecular species at equilibrium, which is evidenced by the plateau phases in the transitions (Fig. 3A). Under these conditions one thus has to postulate the presence of at least one unfolding intermediate (I), the native form (N) and the unfolded protein (U). The equilibrium fractions of N, I and U at pH 4.0 and different urea concentrations, as deduced from a three-state analysis of the transition (25), are shown in Fig. 3B. The analysis shows that the unfolding intermediate is populated to 0.2% at pH 4.0 in the absence of urea, and can be accumulated to 95% in 3.5 M urea (Fig. 3B) (22). Therefore, the unfolding intermediate of *m*PrP(121–231) could be characterized spectroscopically. In contrast to the far-UV CD spectra of native *m*PrP(121–231) at pH 7.0 and pH 4.0, which are α-helical with minima at 222 nm and 208 nm and a mean residue ellipticity of –13600 deg $cm^2 dmol^{-1}$ at 222 nm, the spectrum of the intermediate has a minimum at 215 nm with a mean residue ellipticity of –7000 deg cm^2 $dmol^{-1}$, indicating a high content of β-sheet structure and a strong decline of α-helix content (22) (Fig. 2D).

Within the framework of the "protein-only" hypothesis, observation of this acid-inducible, alternative conformation of *m*PrP(121–231), which shares secondary structural features with PrP^{Sc}, raises the question of its possible involvement in the generation of the infectious prion agent *in vivo*. In this context, it is important to note that natural PrP^{C} appears to be clustered in cholesterol-rich invaginations of the cell membrane, so-called caveolae (26), which may bud from the membrane and fuse with endosomes in a clathrin-independent endocytosis pathway. As the endosomal lumen is the compartment where the insoluble PrP^{Sc} amyloid accumulates in scrapie-infected cells (27), the conversion of PrP^{C} to PrP^{Sc} might occur

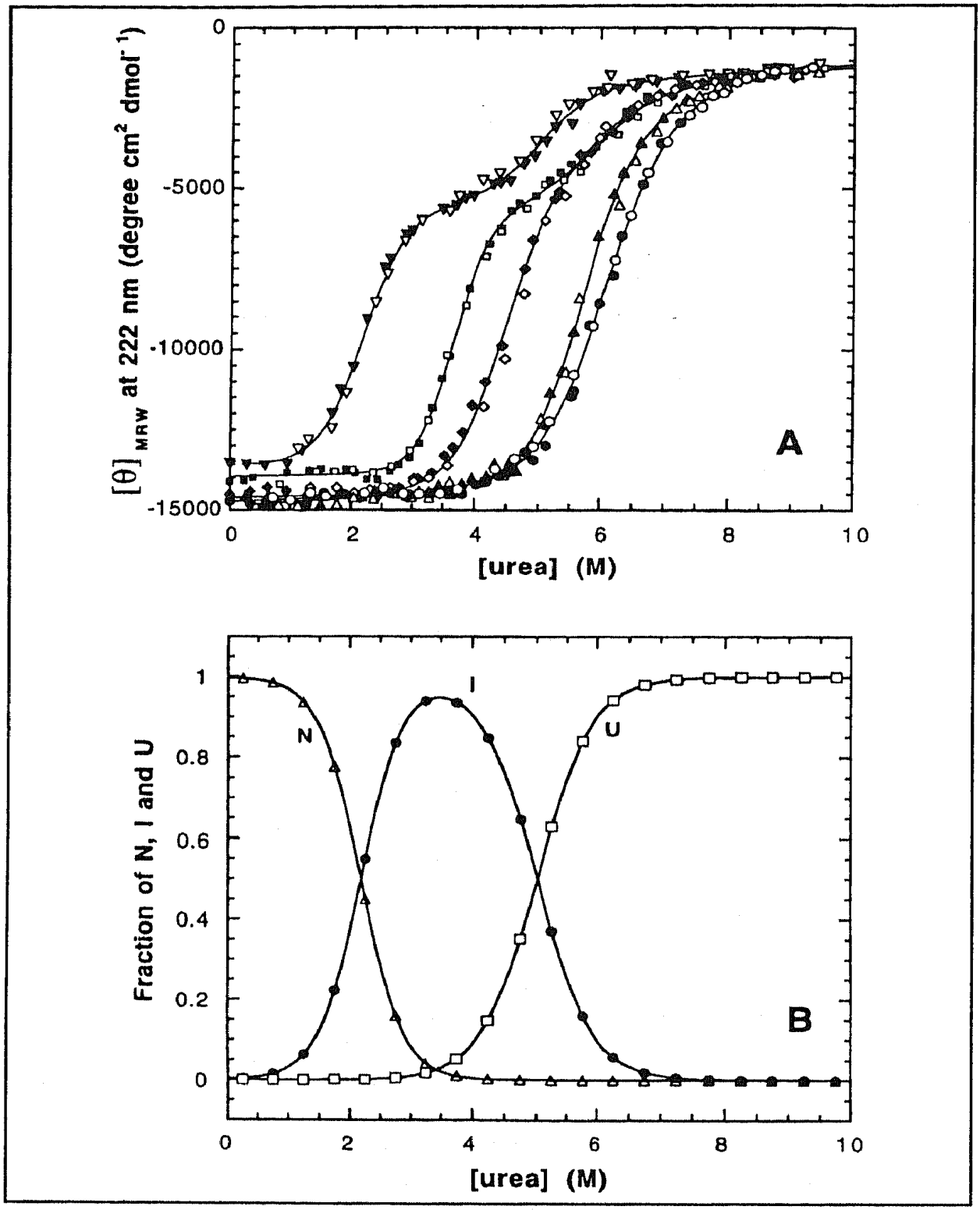

Figure 3. pH-dependence of the urea-induced equilibrium unfolding transitions of *m*PrP(121–231) at constant ionic strength (88 mM) and 22°C. (A) Unfolding transitions at pH 4.0 (▼), 4.5 (■), 5.0 (◆), 6.0 (▲) and 7.0 (●) monitored by the far-UV CD signal at 222 nm. All transitions are completely reversible as the corresponding refolding transitions are identical (open symbols). The transitions at pH 5.0, pH 6.0 and pH 7.0 were analyzed according to the two-state model of folding, the transitions at pH 4.0 and pH 4.5 according to the three-state model of folding (solid lines). (B) Three-state analysis of the urea-dependent equilibrium populations of native (N, Δ) and unfolded (U, ●) *m*PrP(121–231), and of the unfolding intermediate (I, □) at pH 4.0.

during endocytosis. In contrast to physiological pH values at the cell surface, the pH in the endosomal lumen is acidic and varies between 4.0 and 6.0 (28). Therefore, a possible pathway for propagation of the infectious agent would seem to be irreversible incorporation of monomeric PrP^{Sc} precursors induced by acidic pH into pre-exisiting PrP^{Sc} aggregates (Scheme 1):

Scheme 1:

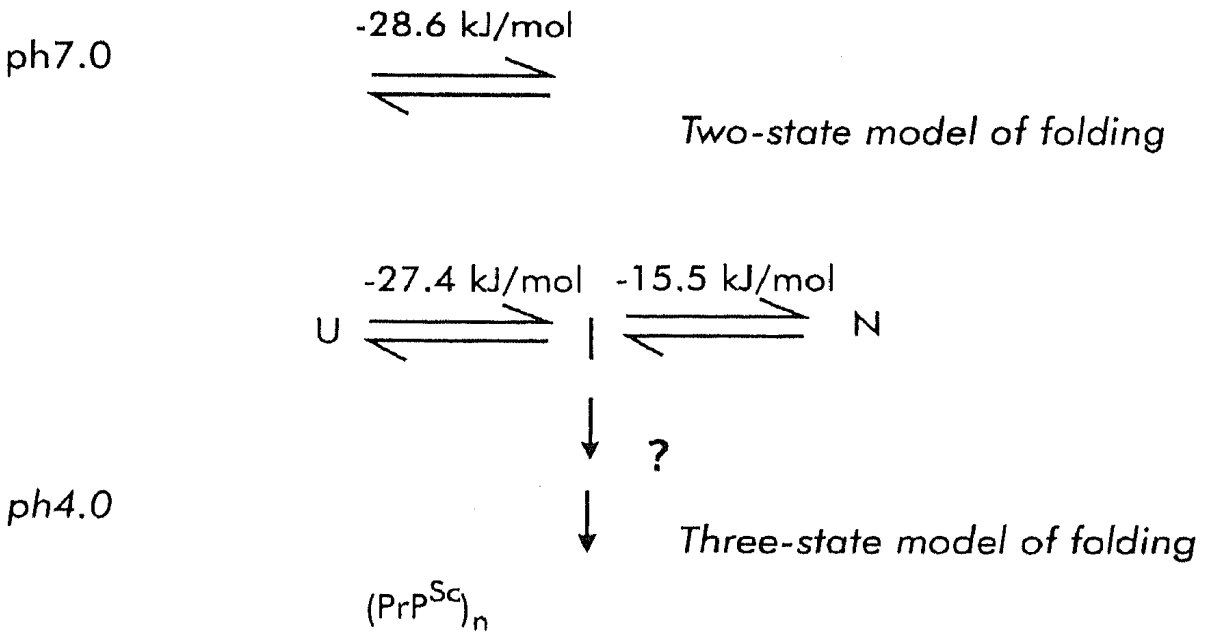

This scheme would be consistent with the nucleation/condensation model for the formation of the infectious PrP^{Sc} oligomer (29), which postulates a fast equilibrium between monomers of PrP^{C} and PrP^{Sc}, and a rate-limiting association of PrP^{Sc} to an oligomer of critical size which acts as nucleus for further incorporation of PrP^{Sc} monomers. The equilibrium between native *m*PrP(121–231) and the intermediate is indeed very rapid and is reached during the dead time of manual mixing (22). Importantly, acidic pH has also been shown to promote the formation of amyloid fibrils of another amyloidogenic protein, transthyretin, which represents the main β-sheet amyloid deposit of familial amyloidotic polyneuropathy (FAP) (30).

So far, the importance of the β-sheet-like equilibrium unfolding intermediate of *m*PrP(121–231) for the formation of the infectious prion agent *in vivo* remains uncertain. An acid-induced β-sheet-like intermediate was however also found for a longer segment of the human prion protein *h*PrP(90–231) (31, 32), demonstrating that formation of the intermediate at acidic pH is independent of the flexible segment 90–120 and an intrinsic property of the C-terminal domain *m*PrP(121–231) (22). The pH-dependence of folding pathway and stability of *m*PrP(121–231) indicates that some of the conformational differences between PrP^{C} and the PrP polypeptide chain in PrP^{Sc} may include the region 121–231. This would be a possible explanation of the finding that the only PrP^{Sc}-specific antibody that is presently available exclusively recognizes regions in the C-terminal domain of the prion protein (33).

The NMR solution structures of the full-length prion protein of the mouse, *m*PrP(23–231), and the C-terminal 111-residue fragment *m*PrP(121–231)

The three-dimensional structures of recombinant murine PrP^C and its isolated 111-residue fragment *m*PrP(121–231) in solution were determined by NMR spectroscopy (20, 21). The structures (Fig. 4) are in agreement with the domain architecture suggested by the aforementioned biochemical experiments. Specifically, the NMR data on murine full-length PrP^C revealed that under the applied experimental conditions, *i.e.*, pH 4.5 and 20 °C in 90% H_2O/10% D_2O, the N-terminal segment 23–125 is extended and flexibly disordered in solution, as evidenced by rotational correlation times below 1 ns for all ^{15}N–^1H moieties. Such short correlation times are typical for "random coil-like" polypeptides (21). In contrast, the C-terminal segment 121–231 of full-length *m*PrP^C possesses the same tertiary structure as that observed for the isolated *m*PrP(121–231) fragment. Very similar results were subsequently reported for the full-length prion protein from Syrian hamster and its fragment 90–231 (34, 35).

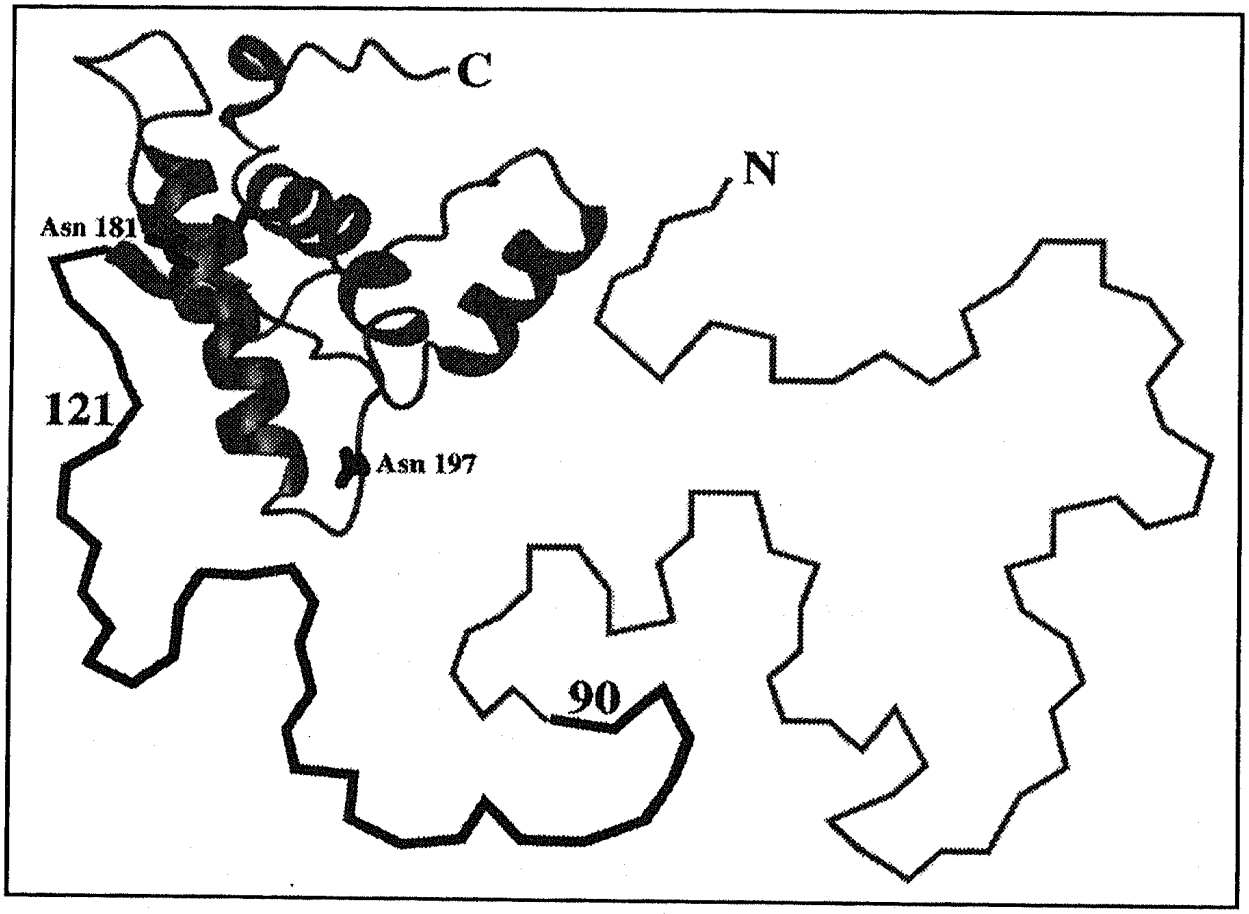

Figure 4. Ribbon diagram of the structure of recombinant murine PrP^C, with the flexibly disordered N-terminal tail comprising residues 23–125 and the folded C-terminal domain *m*PrP(126–231). The disulfide bond Cys179–Cys214 and the side chains of Asn181 and Asn197, which are glycosylated in natural PrP^C, are drawn in black. The segment 90–125, which is flexibly extended in *m*PrP^C but inaccessible for proteases in PrP^{Sc}, is indicated by a thick line. The figure was prepared with the program MOLMOL (51).

The domain *m*PrP(121–231) (Brookhaven Protein Data Bank, accession Nr. 1AG2) possesses a so far unique polypeptide fold (20). It includes three α-helices comprising the residues 144–154, 175–193 and 200–219, a short two-stranded antiparallel β-sheet with residues 128–131 and 161–164, and a short helical segment comprising residues 222–226. The second and the third helix are linked by the single disulfide bond in the protein (Fig. 4). The twisted V-shaped arrangement of these two helices forms the scaffold onto which the β-sheet and the first helix are anchored. *m*PrP(121–231) possesses a hydrophobic core of 20 tightly packed amino acid residues, most of which belong to the helices 2 and 3. This hydrophobic core is surrounded by an "outer shell" of protein structure with 22 hydrogen bonds and salt bridges between amino acid side chains. This outer shell contains the first α-helix and the β-sheet. The side chain hydrogen bonds of this outer shell include medium-range interactions in all three helices and a variety of long-range interactions. The N-terminus of the first helix contains the medium-range hydrogen bond Asn143H^{δ}–O^{ε}Glu146 and the N-terminus of the third helix is stabilized by a capping box (36). Among the

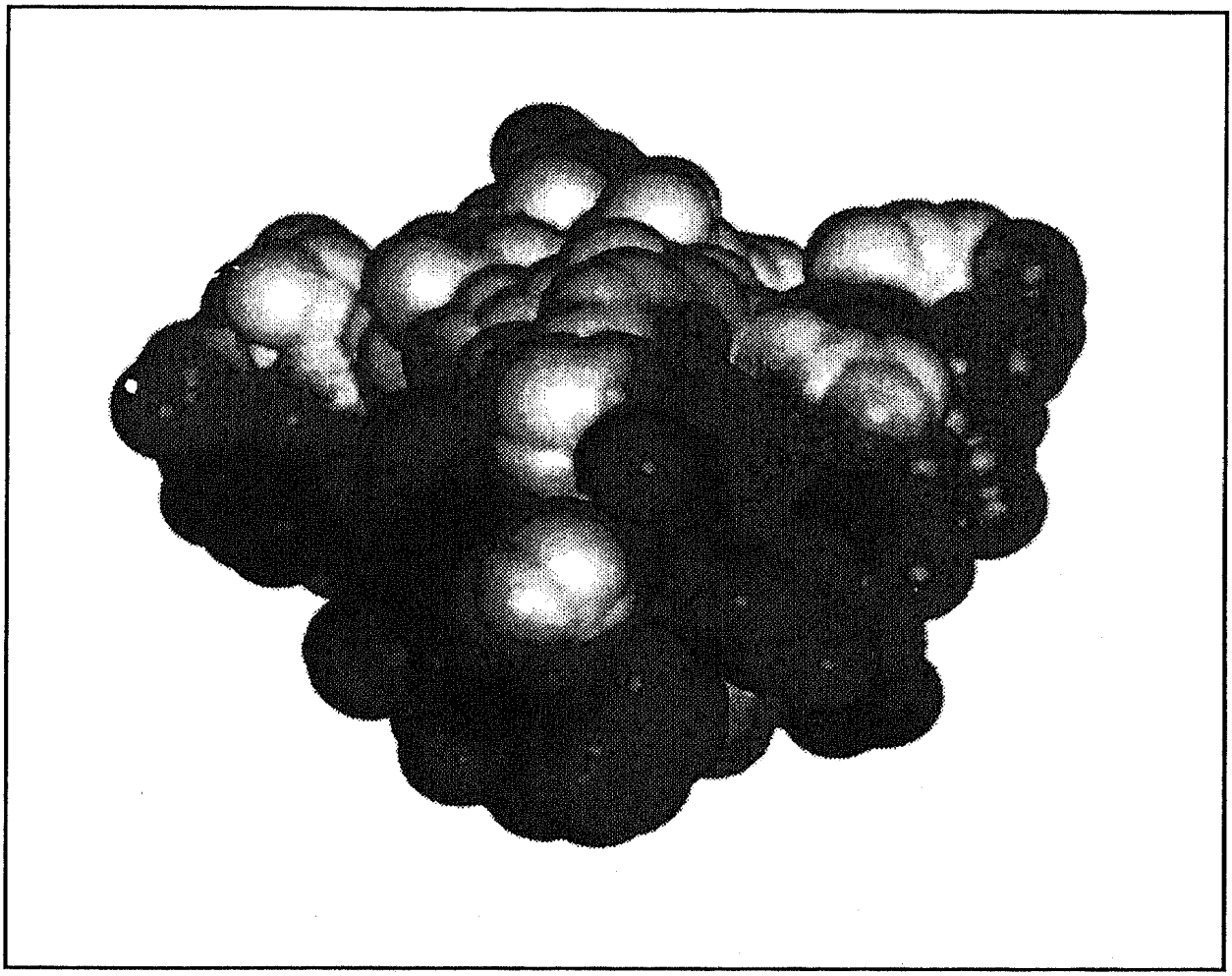

Figure 5. Surface presentation of the energy-refined mean NMR structure of murine PrP(121–231). Grey levels indicate the electrostatic potential, with dark grey for negative charges, and light grey for positive charges. The orientation corresponds to a 90 degree rotation about a vertical axis with regard to the orientation of the domain in Fig. 4.

longer-range hydrogen bonds connecting different groups within the outer shell are the two hydrogen bonds Tyr128H^{η}–O^{δ}Asp178 and Tyr162H^{N}–O^{γ}Thr183 and the salt bridge Arg164–Asp178; these connect the β-sheet with helix 2 (cf. Fig. 8). The salt bridge Arg156–Glu196 is another example of a structurally important contact, as it orients the C-terminal end of helix 1 towards the loop connecting the other two helices. Such a "two-layer architecture", where a shell of hydrogen bonds involving polar side chains surrounds a hydrophobic core, is rather commonly observed in globular proteins. However, *m*PrP(121–231) has a markedly uneven distribution of positively and negatively charged surface residues (Fig. 5). The dipolar character of the domain may be important for the orientation of $mPrP^{C}$ relative to the cell surface in its membrane-anchored form (20), with the positively charged surface, which also includes some hydrophobic patches, probably oriented towards the cell membrane. Both glycosylation sites would then be located on the opposite, solvent-exposed, negatively charged surface (Fig. 4).

In a search for structural similarities between *m*PrP(121–231) and other proteins in the database the distance matrix algorithm implemented in the program DALI (37) indentified the only close match for the hemoglobin of the marine bloodworm (38). A reasonable structural fit was obtained when the first, sixth and seventh helix of this hemoglobin were superimposed with the helices 1, 2 and 3 in *m*PrP(121–231).

Structural and biochemical analysis of amino acid replacements in the prion protein that have been related to inherited human TSEs

The domain *m*PrP(121–231) contains 8 out of 11 amino acid replacements in the mature prion protein that have been shown to segregate with familial human prion diseases, *i.e.*, familial CJD, Gerstmann-Sträussler-Scheincker syndrome (GSS) and fatal familial insomnia (FFI) (5) (Fig. 6). A previously formulated hypothesis suggested a uniform mechanism for the impact of all 11 variants, according to which these amino acid substitutions would destabilize the three-dimensional structure of PrP^{C} and thereby facilitate its conversion into PrP^{Sc} (16, 39, 40). Here, we used *m*PrP(121–231) as a model system to analyze likely impacts of individual ones of these disease-related amino acid exchanges on the structure and stability of human PrP^{C}. The 8 exchange sites contained in PrP(121–231) are identical in wild type human and mouse PrP, and the residues that form direct contacts with these amino acids in the structure of *m*PrP(121–231) are also the same in human and mouse PrP.

We introduced all eight specific point mutations individually into the gene coding for *m*PrP(121–231) and produced the corresponding variants in the periplasm of *E. coli*. Four variants with Val180Ile, Glu200Lys, Arg208His and Val210Ile were obtained as soluble proteins in the periplasmic fractions, with yields comparable to wild type *m*PrP(121–231) (Fig.7). The same holds for the Met129Val variant. In contrast, the variants with Asp178Asn, Met129Val/Asp178Asn, Thr183Ala, Phe198Ser and Gln217Arg exclusively accumulated in insoluble inclusion bodies. Since the expression yield in the periplasm of *E. coli* has been reported to correlate

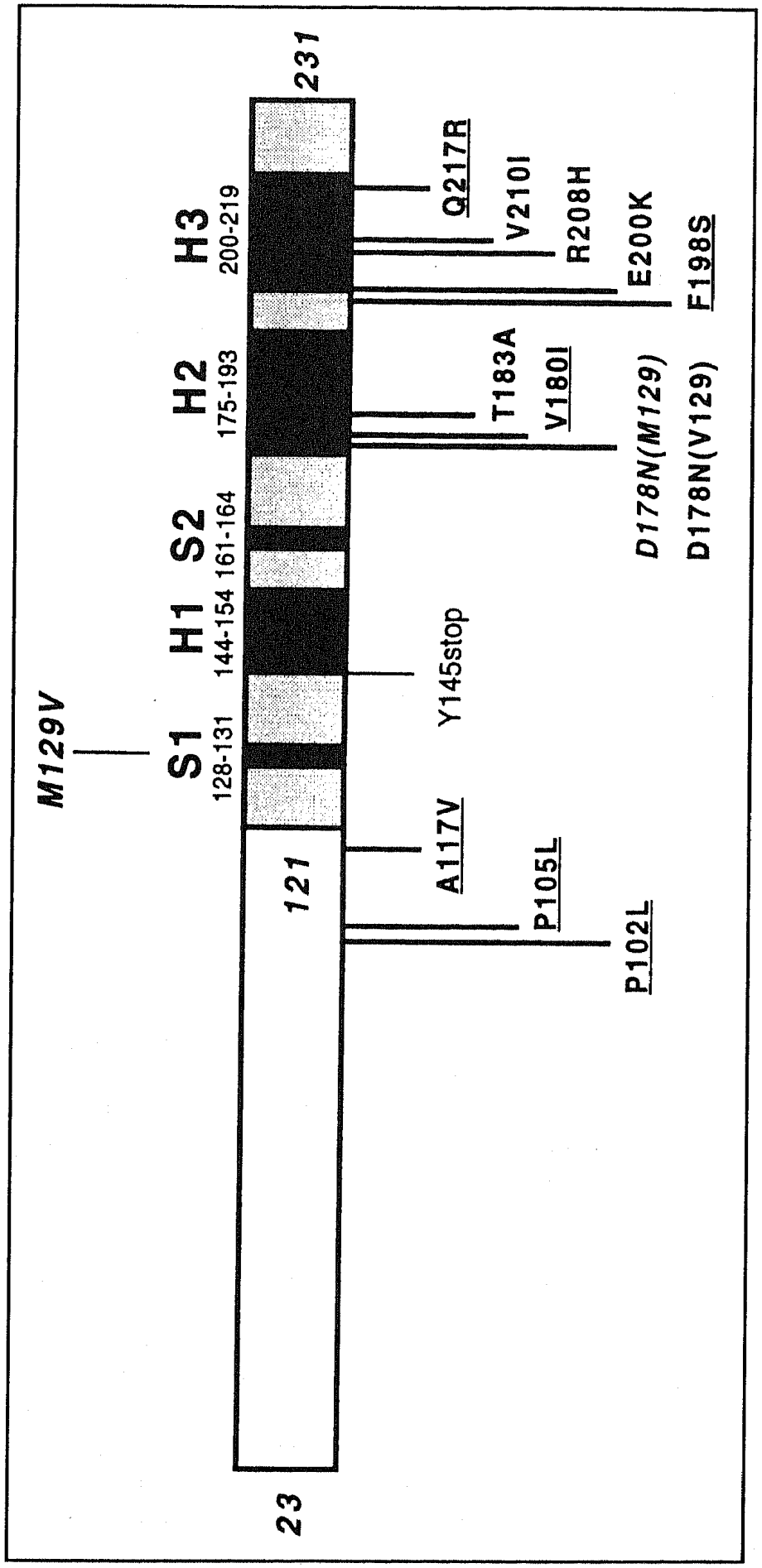

Figure 6. Sequence locations of point mutations in human PrP that have been associated with inherited human TSEs (5). The positions of the three α-helices (H1, H2, H3) and both strands of the antiparallel β-sheet (S1, S2) in the folded C-terminal domain are indicated as black rectangles. Amino acid exchanges segregating with inherited CJD, FFI (italics) and GSS (underlined) are shown in the lower part of the figure. All exchanged residues are identical in wild type human and mouse PrP. The polymorphism at residue 129 in human PrP, which determines the phenotype of the diseases related with the D178N mutation, is indicated above the sequence. The figure was prepared with the program MOLMOL (51).

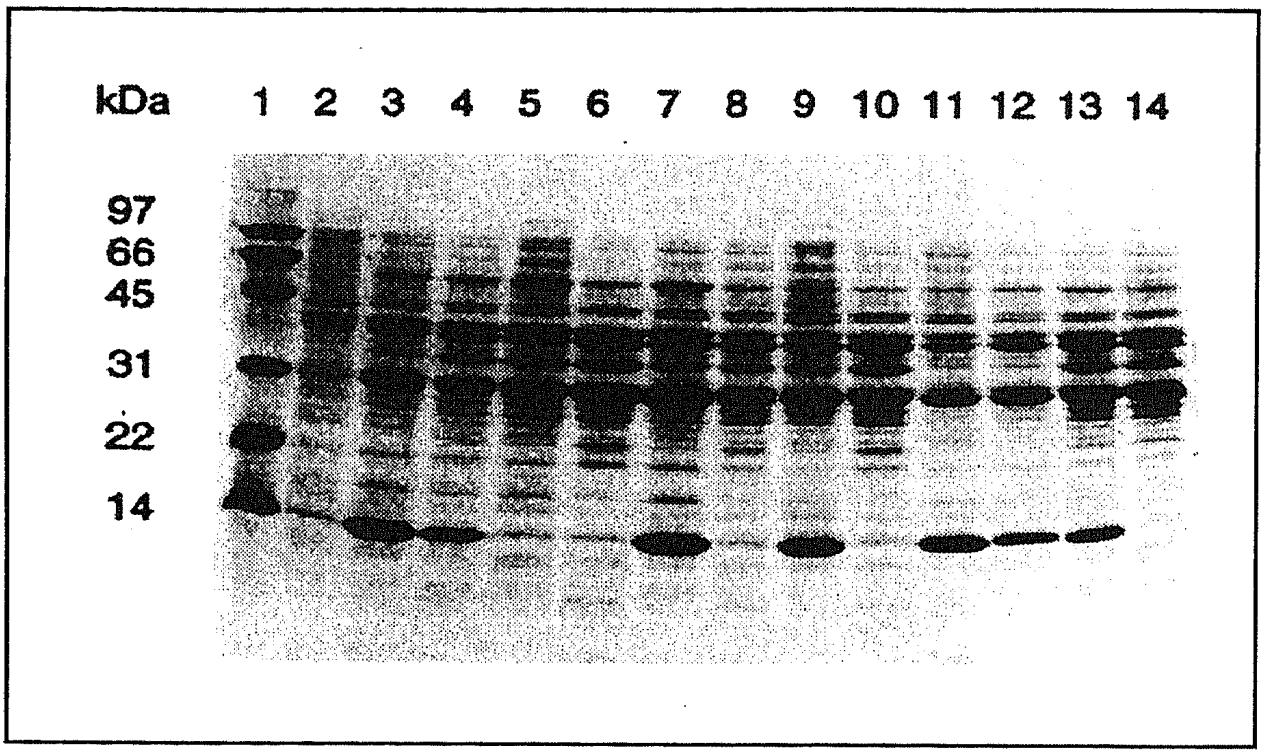

Figure 7. Soluble periplasmic fraction of *E. coli* BL21(DE3) cells expressing wild type and mutant murine PrP(121–231). A Coomassie-stained SDS-polyacrylamide gel (15% w/v) is shown. 1, molecular mass standard; 2, wild type PrP(121–231) before induction with IPTG; 3, wild type PrP(121–231) 18 hours after induction (same as for the variants shown in the following lanes); 4, Met129Val; 5, Asp178Asn; 6, Met129Val/Asp178Asn; 7, Val180Ile; 8, Thr183Ala; 9, Thr190Val; 10, Phe198Ser; 11, Glu200Lys; 12, Arg208His; 13, Val210Ile; 14, Gln217Arg. The exchanges Met129Val and Thr190Val correspond to natural polymorphisms in human and murine PrP, respectively. The band at approximately 14 kDa corresponds to *m*PrP(121–231).

with protein stability (41), two different classes of mutations can be distinguished on the basis of these experiments. One class comprises the soluble proteins with wild type-like stabilities, and the other class is represented by the insoluble variants whose stability is likely to be significantly reduced. This classification has been confirmed by thermodynamic measurements, which revealed that the variants that were obtained in inclusion bodies in the periplasm have indeed the lowest stability of all mutant proteins (S. Liemann and R. Glockshuber, submitted).

The 8 disease-related amino acid replacements within the polypeptide segment 121–231 are all located within or sequentially adjacent to the helices 2 and 3. The mutation sites related to the human disease phenotypes GSS and CJD do not form clusters in the structure of *m*PrP(121–231). It can thus be excluded that there are GSS- and CJD-specific subdomains in PrP^C that would be responsible for the development of these disease phenotypes. For most of the amino acid replacements that lead to insoluble *m*PrP(121–231) in the periplasm of *E. coli* the reduced stability can quite readily be rationalized by the three-dimensional structure of PrP^C. For example, the mutation Asp178Asn removes the salt bridge Asp178–Arg164 (Fig. 8), which is highly conserved in the prion proteins of mammalian species (10, 11). Similarly, the mutation Thr183Ala (Fig. 8) eliminates two hydrogen bonds that es-

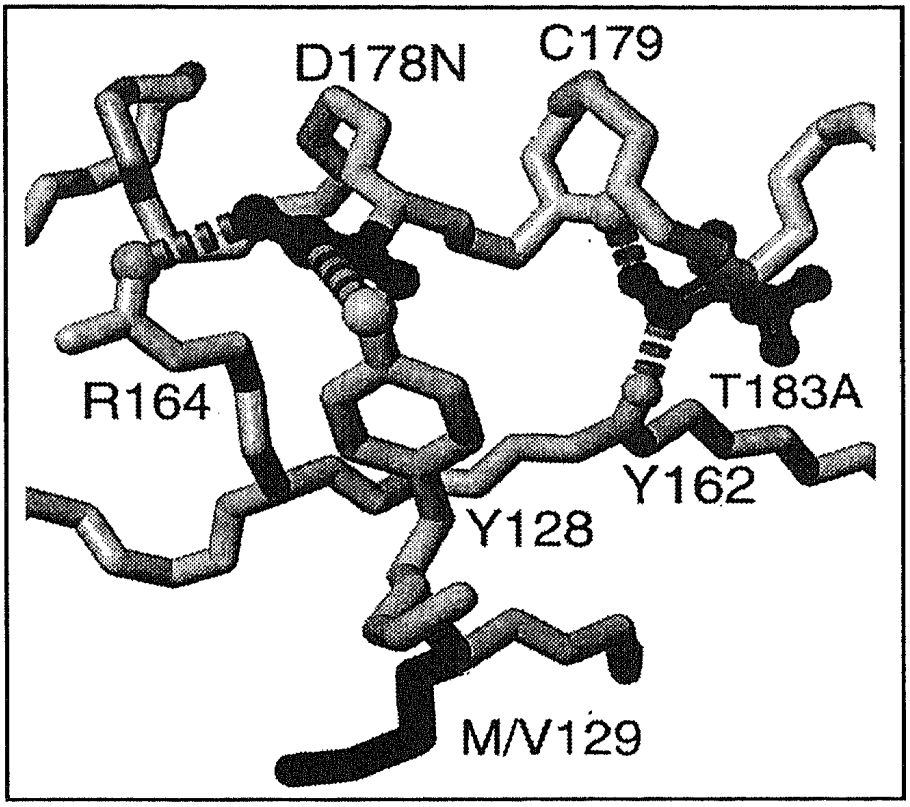

Figure 8. Locations in the energy-refined mean NMR structure of *m*PrP(121–231) of the point mutation sites Asp178Asn and Thr183Ala that have been associated with inherited CJD. Color code: grey, polypeptide backbone represented by the bonds linking the heavy atoms N, C^{α} and CÕ, and side chains of Arg164 and Tyr128; black, side chains of the point mutation sites Asp178 and Thr183 and the polymorphism site Met/Val129 in human PrP. In all instances the underlined residues are shown, which are those found in wild type *m*PrP. Hydrogen bonds are represented by broken dark grey cylinders. The figure was prepared with the program MOLMOL (51).

tablish a side chain-mediated link between helix 2 and the β-sheet, *i.e.*, Thr183$O^{H\gamma}$–O^{δ}Cys179 and Tyr162H^{N}–O^{g}Thr183, and the mutation Glu217Arg eliminates a hydrogen bond with the carbonyl oxygen of Ala133. The replacement Phe198Ser causes a major disruption of side chain packing, so that the reduced stability of the mutant protein does not come as a surprise. On the other hand, only minor effects on protein stability are expected from the structural analysis of the other point mutations. For example, for the replacements of Val by Ile in either of the positions 180 or 210 there is enough space to accommodate the somewhat larger Ile side chains without major rearrangement of other side chains.

Overall, the amino acid replacements that appear, from inspection of the three-dimensional structure, most likely to destabilize the structure of *m*PrP(121–231) lead to insoluble inclusion bodies upon periplasmic expression in *E. coli* and lower thermodynamic stabilities, while the variants for which only minor changes in protein stability are predicted are obtained as soluble proteins in the bacterial periplasm with similar stabilities as wild type *m*PrP(121–231). Thus, destabilization of PrP^{C} cannot be a general mechanism underlying the easier formation of the infectious scrapie agent in inherited human prion diseases. The same conclusion comes from

the fact that the three point mutations at residues 102, 105 and 117, which all segregate with inherited GSS (Fig. 6), are located in the unstructured region of PrP^C and are thus unlikely to affect the thermodynamic stability of PrP^C. Therefore, other mechanisms for the development of inherited human TSEs caused by point mutations in the PrP gene need to be considered, for example, altered glycosylation patterns, increased stability of the variant PrP^{Sc} forms, or accelerated kinetics of PrP^{Sc} formation from the variant proteins. This view is supported by studies on the expression of the variants Pro102Leu, Asp178Asn/Met129, Glu200Lys and Thr183Ala of the full-length murine prion protein in cultured cells (42–44). While the variant Thr183Ala failed to reach the cell surface, possibly due to elimination of the glycosylation site at Asn181, biochemical properties similar to those of PrP^{Sc} were observed for the other mutant proteins, in particular insolubility, protease resistance and aberrant membrane attachment (42–44). The mutation Glu200Lys, which led to insoluble PrP in the cell culture experiments but did not affect solubility of *m*PrP(121–231) in the bacterial periplasm (Fig. 7), demonstrates rather clearly that factors other than reduced stability of the mutant proteins must play a role in promoting formation of PrP^{Sc} *in vivo*.

Structural basis for the role of the polymorphism Met/Val129 in the human prion protein

Considering the proposed increase in the β-sheet content in PrP during the transition from PrP^C to PrP^{Sc} (8, 9) we propose that the short β-sheet in *m*PrP(121–231) might be a nucleation site for a conformational transition that could include the polypeptide segment 90–127, and possibly the loops connecting the β-sheet to the first helix, which is predominantly hydrophilic and does not show amphipathic character (20). The β-sheet contains the human polymorphism Met/Val129, and homozygosity with respect to this position has been correlated with increased incidence of spontaneous CJD and vCJD (5, 45). Furthermore, in homozygotes the nature of residue 129 determines the phenotype of the inherited disease that segregates with the Asp178Asn mutation, *i.e.*, either CJD or FFI (46). Although there is no direct contact between the side chains of residues 129 and 178, two hydrogen bonds in wild type *m*PrP(121–231) link the side chain of Asp178 with two side chains in the β-sheet, one of which is directly adjacent to position 129 (Fig. 8). The perturbation by the Asp178Asn mutation of the hydrogen bonding network involving Arg164, Tyr128 and Asp178 may thus be modulated by the nature of the amino acid residue in position 129, which would be manifested by different disease phenotypes for the two combinations Asn178/Met129 and Asn178/Val129. The specific interaction between positions 129 and 178 in the NMR structure also provides a rationale for the observation that the Met/Val129 polymorphism does not affect the phenotypes of the inherited prion diseases that segregate with any of the other mutations.

Structural aspects of the species barrier for transmission of prion diseases

This section correlates biological and biochemical data on the observed species barrier of TSEs (4, 5) with the NMR structure of *m*PrP(121–231). Within the framework of the "protein-only" hypothesis, the probability of transmission of prion-related encephalopathies between different species is governed by the differences in primary structure between their prion proteins. These differences in primary structure may affect transmissibility in various ways, for instance by modulation of the affinity of PrP^{C} for PrP^{Sc} from another species, or by interference with the oligomerization of PrP^{Sc}. Therefore, mapping of the amino acid replacements onto the three-dimensional structure of the prion protein domain *m*PrP(121–231) should provide a better understanding for possible roles of individual exchanges for the transmission of prion diseases between different species.

Amino acid replacements in mammalian prion sequences

Large parts of PrP(121–231) are not affected by species variations: the β-sheet (the only amino acid replacement is strictly conservative), the loop linking the helices 2 and 3, and several turns from each of the helices (Fig. 9). Conservation of these molecular regions may be required for maintaining the protein fold, or in some cases they may also serve to form additional intermolecular interactions, for example, with the cell surface to which the protein is attached. Nonetheless, a comparison of 23 mammalian prion protein sequences shows 18 positions with relevant amino acid replacements (Fig. 9) (11). These were grouped into four classes A–D on the basis of their locations in the three-dimensional structure (Fig. 10). The class A sites form a dense cluster of nine mostly polar residues in the loop connecting the second β-strand with the second helix (residues Arg164, Val166, Gln168, Ser170 and Asn174), and near the end of helix 3 (residues Val215, Gln219, Lys220 and Gln223). Class B includes the five hydrophobic residues Met138, Ile139, Ile184, Val203 and Met205 in the interface between the first helix and the remainder of the protein. Class C contains the positions of Trp145 and Tyr155 at the two ends of the first helix, which are filled with aromatic residues in most species (Fig. 9), and Asn143, which precedes this helix. Finally, class D is the single exchange Gln186Glu found in the bovine protein, which introduces a negative charge in an otherwise conserved surface region.

A potential protein binding site formed by polar and charged residues

In class A the amino acid replacements at positions 168, 219, 220 and 223 involve changes in the electrostatic charge of the side chains (Fig. 9). These may modify

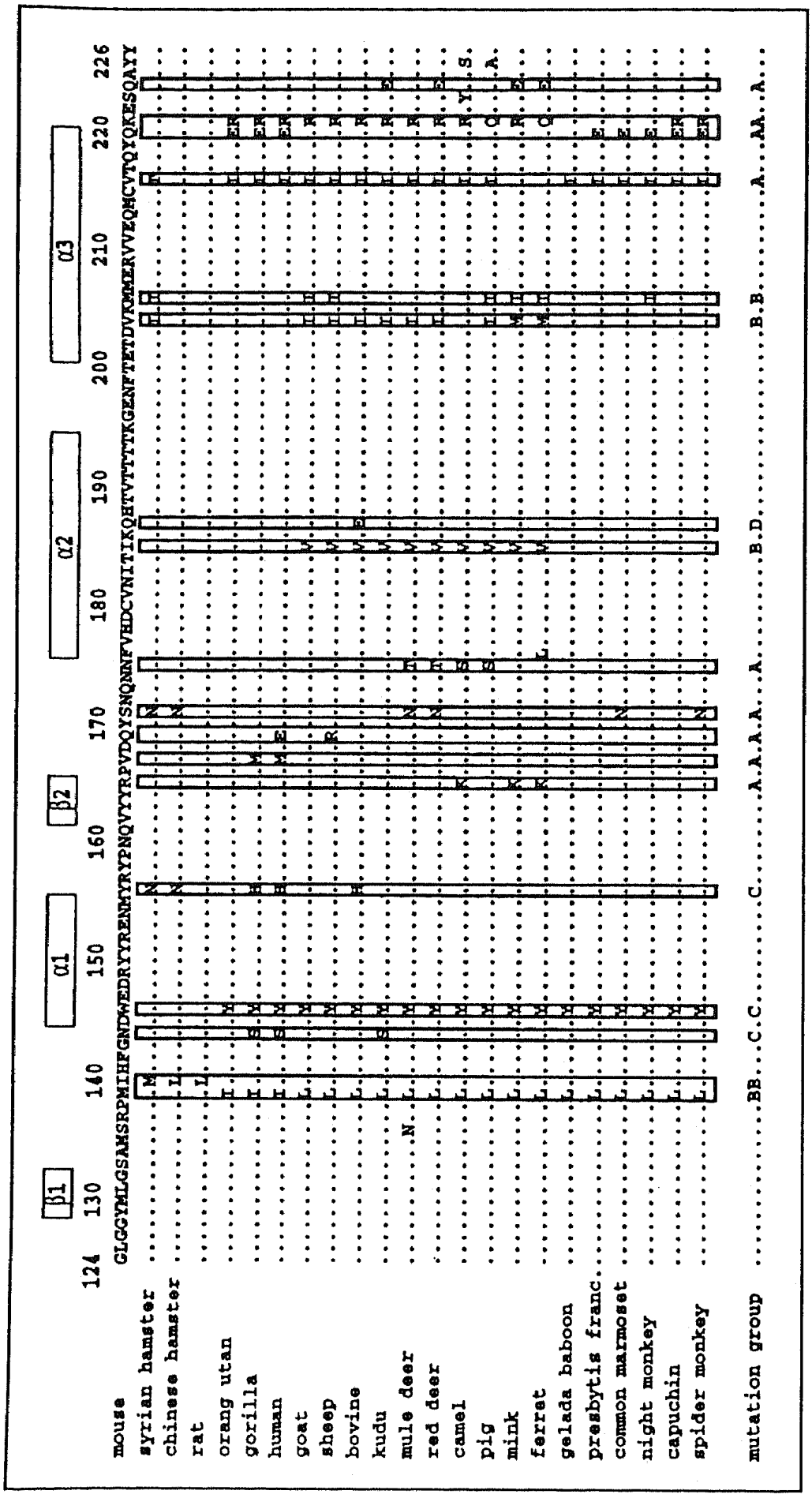

Figure 9. Sequence comparisons of the fragment 124–226 of mammalian prion proteins (see text for the selection criteria used), with the mouse sequence at the top. The sequence numbers refer to the residue under the third digit. The locations of the regular secondary structures in *m*PrP(121–231) are indicated above the mouse sequence. Sequence positions with relevant residue variations are indicated by vertical boxes and classified into four groups A, B, C and D (see text).

long-range forces effective in intermolecular recognition. Thus, the total charge of the two fragments with residues 161–170 and 214–226 is –1 in *m*PrP and in the bovine prion protein, –3 in human PrP and 0 in the sheep protein. In addition, the substitution of further polar residues alters the protein surface in this region, and modulates the hydrogen bonding propensity for interactions with any molecule that may dock to PrP^C in this region. Thus, the class A residues make this region a likely candidate for a specific protein–protein interaction site (11). Independently, several residues in this molecular region were suggested to be involved in recognition of "protein X", a hypothetical cofactor that might be involved in the PrP^C to PrP^{Sc} transformation (48, 49). This molecular region contains also two of the three peptide segments that constitute the epitope for a recently described PrP^{Sc}-specific monoclonal antibody (33).

Amino acid replacements of hydrophobic and aromatic residues

In the prion proteins shown in Fig. 9, the type B sites contain exclusively hydrophobic side chains of Val, Leu, Ile or Met. Because of their limited surface accessibility, the molecular region containing these residues is not reminiscent of a potential binding site for other molecules interacting with folded PrP^C. However, upon limited conformational rearrangement of PrP^C, for example, by unfolding of the helix 1 (20), several of these hydrophobic residues would become accessible and could thus support self-association of PrP. The observation in the spatially neighboring positions 184 and 203 that replacement of Ile184 by Val correlates in all but two species with the replacement of Val203 by Ile or Met (Fig. 9) appears to further support that class B amino acid exchanges leave the PrP^C surface properties largely unperturbed.

In this context it is intriguing that it has been suggested that substitution of Met139 in Syrian hamster PrP by the Ile side chain present in mouse PrP might be sufficient to protect hamster from infection by mouse PrP^{Sc} (50). This would place a critical structural feature for the species barrier in the interface between helix 1 and the protein core (Fig. 10), and the implication is that residue 139 would become operational only after initial conformational transitions of PrP^C induced, for example, by complexation with PrP^{Sc} and possibly with "protein X".

The group C sites are related to a special feature of helix 1, namely the partial solvent-exposure of four aromatic side chains in the mouse sequence. With the sole exception of Met154 all other side chains of this helix have polar character, and the positions 146–148, 151 and 152 actually contain charged side chains (Fig. 9). The combination of long-range electrostatic potentials, high hydrogen bonding propensity and the presence of exposed aromatic residues on the solvent-accessible surface of helix 1 again represents structural features of a surface area that could well function as a species-specific recognition site for other proteins. In particular, the substitution of the unusual surface-exposed Trp145 can be expected to modify the specificity of intermolecular interactions in this molecular region, which thus becomes a possible site for interactions with infectious PrP^{Sc}.

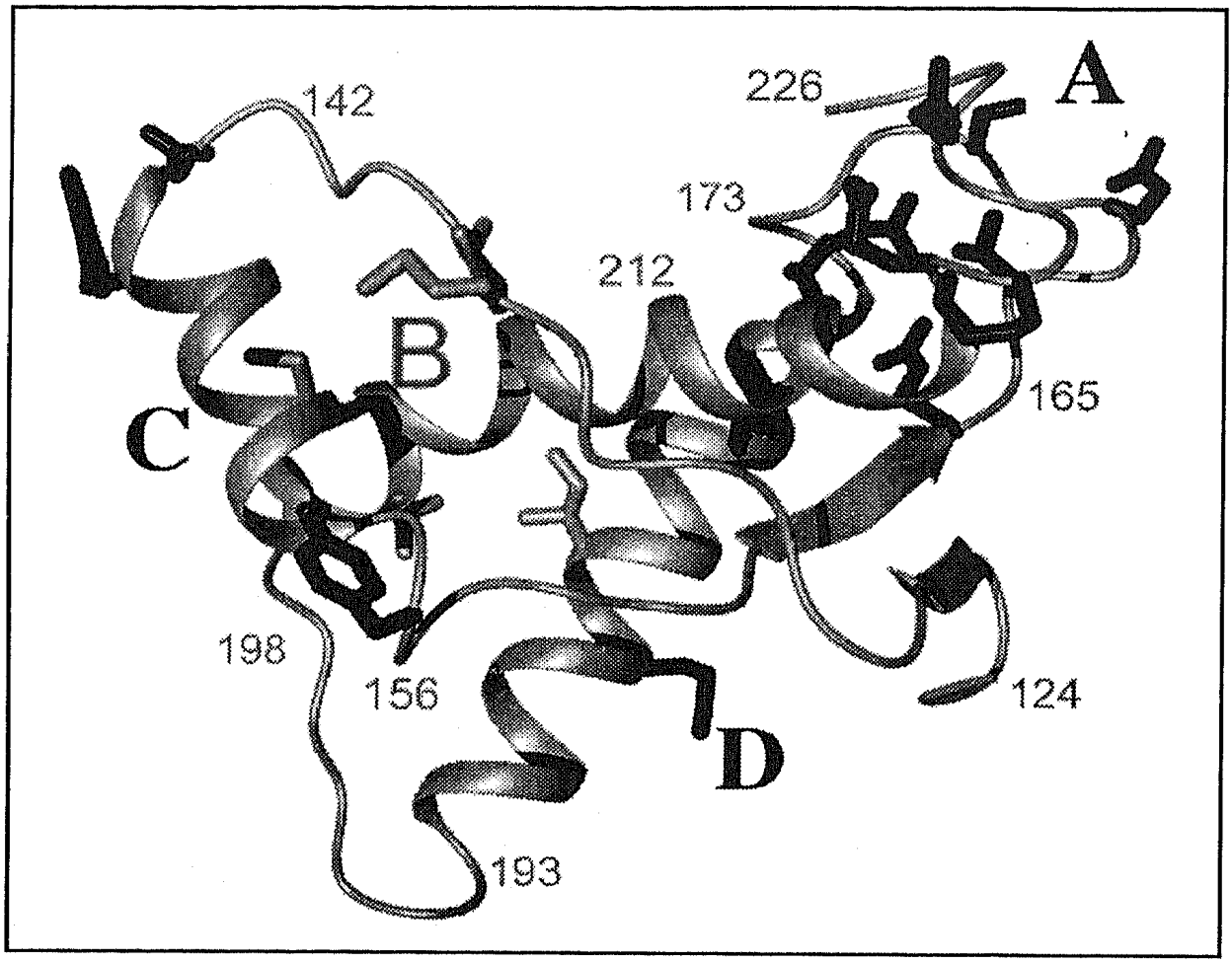

Figure. 10. Location of the variable residues in mammalian prion proteins (Fig. 9) in the energy-refined mean NMR structure of *m*PrP(121–231). The backbone is shown as a smooth ribbon representing a spline function through the α-carbon positions. Side chains of the mouse prion protein corresponding to variable residues are black for classes A, C and D, and grey for class B. Selected positions in the sequence are identified by numbers, and the spatial regions containing the class A to D sites (see Fig. 9) are indicated by capital letters. The figure was prepared with the program MOLMOL (51).

A further variable surface area in the bovine prion protein

The class D exchange Gln186Glu in bovine PrP introduces a negative electrostatic charge in a surface location that is clearly separated in space from the positions of the classes A, B and C (Fig. 10). Recent results indicate the presence of Glu186 also in the related species Watussi, Banteng and Wisent (H. Schätzl, personal communication). Interestingly, the newly determined prion protein sequences of the house dog, the canadian wolf and the dingo (H. Schätzl, personal communication) further extend the available information on D-type mutation sites, since in these species the otherwise strictly conserved Asn159 (Fig. 9) is replaced by Asp, and this negative charge is located in close spatial proximity to position 186 (Fig. 10). Thus, a third variable surface area in PrP^C might emerge by further extension of the sequence data base (11). This site might be functional in the species barrier with cattle, including possibly also transmission of disease from BSE-infected cows to other species.

1.8. Conclusions

At the present stage, the most important result from the three-dimensional structure of $m\mathrm{PrP}^{C}$ is that it defines a minimal structural rearrangement that must occur during formation of PrP^{Sc} from PrP^{C}: Since the entire fragment 90–231 is resistant to protease digestion in PrP^{Sc} (4, 5), the segment 90–125, which is flexible in PrP^{C}, must undergo a significant conformational change that reduces its accessibility for proteases.

For future work, the three-dimensional structure of murine PrP^{C} provides a platform for the rational design of *in vitro* and *in vivo* experiments on the biological function of PrP^{C} and the mechanisms underlying the propagation of prions. By analogy with other areas of biomedical research it can be expected that structure-based rational thinking will support the continued search for reliable diagnosis and treatment of TSEs.

Acknowledgements

We thank Drs. A. Aguzzi, B. Oesch and C. Weissmann for discussions, and Dr. H. Schätzl for communicating results prior to publication. Financial support was obtained from the ETH Zürich, the Schweizerische Nationalfonds (Projects 31.49047.96 and 438+.050285 (K.W.), and 438+.050287 (R.G.)), and the Boehringer-Ingelheim-Fonds (predoctoral fellowship to S.H.).

References

1. Alper, T., Cramp, W.A., Haig, D.A. and Clarke, M.C. 1967. Does the agent of scrapie replicate without nucleic acid? Nature 214: 764–766.
2. Griffith, J.S. 1967. Self-replication and scrapie. Nature 215: 1043–1044.
3. Prusiner, S.B. 1982. Novel proteinaceous infectious particles cause scrapie. Science 216: 136–144.
4. Weissmann, C., Fischer, M., Raeber, A., Büeler, H., Sailer, A., Shmerling, D., Rülicke, T., Brandner, S. and Aguzzi, A. 1996. The role of PrP in pathogenesis of experimental scrapie. Cold Spring Harbor Symp. Quant. Biol. 61: 511–522.
5. Prusiner, S.B. 1997. Prion diseases and the BSE crisis. Science 278: 245–250.
6. Horwich, A.L. and Weissman, J.S. 1997. Deadly conformations–protein misfolding in prion disease. Cell 89: 499–510.
7. Anfinsen, C.B. 1973. Principles that govern the folding of protein chains. Science 181: 223–230.
8. Caughey, B.W., Dong, A., Bhat, K.S., Ernst, D., Hayes, S.F. and Caughey, W.S. 1991. Secondary structure analysis of the scrapie-associated protein PrP 27–30 in water by infrared spectroscopy. Biochemistry 30: 7672–7680.
9. Pan, K.M., Baldwin, M., Nguyen, J., Gasset, M., Serban, A., Groth, D.,

Mehlhorn, I., Huang, Z., Fletterick, R.J., Cohen, F.E. and Prusiner, S.B. 1993. Conversion of α-helices into β-sheets features in the formation of the scrapie prion proteins. Proc. Natl. Acad. Sci. USA 90: 10962–10966.

10. Schätzl, H. M., Da Costa, M., Taylor L., Cohen F.E. and Prusiner, S.B. 1995. Prion protein gene variation among primates. J. Mol. Biol. 245: 362–374.
11. Billeter, M., Rick, R., Wider, G., Hornemann, S., Glockshuber, R. and Wüthrich, K. 1997. Prion protein NMR structure and species barrier for prion diseases. Proc. Natl. Acad. Sci. U.S.A. 94: 7281–7285.
12. Stahl, N. and Prusiner, S.B. 1991. Prions and prion proteins. FASEB J. 5: 2799–2807.
13. Mehlhorn, I., Groth, D., Stöckel, J., Moffat, B., Reilly, D., Yansura, D., Willett, W.S., Baldwin, M., Fletterick, R., Cohen, F.E., Vandlen, R., Henner, D. and Prusiner, S.B. 1996. High-level expression and characterization of a purified 142 residue polypeptide of the prion protein. Biochemistry 35: 5528–5537.
14. Hornemann, S., Korth, C., Oesch, B., Riek, R., Wider, G., Wüthrich, K. and Glockshuber, R. 1997. Recombinant full-length murine prion protein, mPrP(23–231): Purification and spectroscopic characterization. FEBS Lett. 413: 277–281.
15. Zahn, R., von Schroetter, C. and Wüthrich, K. 1997. Human prion proteins expressed in *Escherichia coli* and purified by high-affinity column refolding. FEBS Lett. 417: 400–404.
16. Huang, Z., Gabriel, J.-M., Baldwin, M.A., Fletterick, R.J., Prusiner, S.B. and Cohen, F.E., 1994. Proposed three-dimensional structure for the cellular prion protein. Proc. Natl. Acad. Sci., U.S.A. 91: 7139–7143.
17. Hornemann, S. and Glockshuber, R. 1996. Autonomous and reversible folding of a soluble amino-terminally truncated segment of the mouse prion protein. J. Mol. Biol. 261: 614–618.
18. Price, N.C. and Johnson, C.M. 1993. Proteinases as probes of conformation of soluble proteins. In: Proteolytic Enzymes, A Practical Approach. R.J. Beynon and J.S. Bond, eds. IRL Press, Oxford. p. 163–180.
19. Glockshuber, R., Hornemann, S., Riek, R., Wider, G., Billeter, M. and Wüthrich, K. 1998. Autonomous folding and three-dimensional structure of the carboxy-terminal domain of the mouse prion protein, PrP(121–231). In: Prions and Brain Diseases in Animals and Humans. D.R.O. Morrison and J. Collinge, eds., Plenum Publishing Company, London, in press.
20. Riek, R., Hornemann, S., Wider, G., Billeter, M., Glockshuber, R. and Wüthrich, K. 1996. NMR structure of the mouse prion protein domain PrP(121–231). Nature 382: 180–182.
21. Riek, R., Hornemann, S., Wider, G., Glockshuber, R. and Wüthrich, K. 1997. NMR characterization of the full-length recombinant murine prion protein, mPrP(23–231). FEBS Lett. 413: 282–288.
22. Hornemann, S. and Glockshuber, R. 1998. A scrapie-like unfolding intermediate of the prion protein domain PrP(121–231) induced by acidic pH. Proc.

Natl. Acad. Sci. USA 95: 6010-6014.

23. Pace, C.N. 1986. Determination and analysis of urea and guanidine hydrochloride denaturation curves. Methods Enzymol. 131: 266–280.
24. Prusiner, S.B., Groth, D., Serban, A., Stahl, N. and Gabizon, R. 1993. Attempts to restore scrapie infectivity after exposure to protein denaturants. Proc. Natl. Acad. Sci. USA 90: 2793–2797.
25. Barrick, D. and Baldwin, R.L. 1993. Three-state analysis of sperm whale apomyoglobin folding. Biochemistry 32: 3790–3796.
26. Vey, M., Pilkuhn, S., Wille, H., Nixon, R., DeArmond, S.J., Smart, E.J., Anderson, R.G.W., Taraboulos, A. and Prusiner, S.B. 1996. Subcellular colocalization of the cellular and scrapie prion proteins in caveolae-like membraneous domains. Proc. Natl. Acad. Sci. USA 93: 14945–14949.
27. Arnold, J.E., Tipler, C., Laszlo, L., Hope, J., Landon, M. and Mayer, R.J. 1995. The abnormal isoform of the prion protein accumulates in late-endosome-like organelles in scrapie-infected mouse brain. J. Pathology 176: 403–411.
28. Lee, R.J., Wang, S. and Low, P.S. 1996. Measurements of endosome pH following folate receptor-mediated endocytocis. Biochim. Biophys. Acta 1312: 237–242.
29. Jarrett, J.T. and Lansbury, Jr., P.T. 1993. Seeding "one-dimensional crystallization" of amyloid: a pathogenic mechanism in Alzheimer's disease and scrapie? Cell 73: 1055–1058.
30. Lai, Z., Colon, W. and Kelly, J.W. 1996. The acid-mediated denaturation pathway of transthyretin yields a conformational intermediate that can self-assemble into amyloid. Biochemistry 35: 6470–6482.
31. Swietnicki, W., Peterson, R., Gambetti, P. and Surewicz, W.K. 1997. pH-dependent stability and conformation of the recombinant human prion protein PrP(90–21). J. Biol. Chem. 272: 27517–27520.
32. Zhang, H., Stöckel, J., Mehlhorn I., Groth, D., Baldwin, M., Prusiner, S.B., James, T.L. and Cohen, F.E. 1997. Physical studies of the conformational plasticity in a recombinant prion protein. Biochemistry 36: 3543–3553.
33. Korth, C., Stierli, B., Streit, P., Moser, M., Schaller, O., Fischer, R., Schulz-Schaeffer, W., Kretzschmar, H., Raeber, A., Braun, U., Ehrensberger, F., Hornemann, S., Glockshuber, R., Riek, R., Billeter, M., Wüthrich, K. and Oesch, B. 1997. Prion (PrP^{Sc})-specific epitope defined by a monoclonal antibody. Nature 390: 74–77.
34. James, T.L., Liu, H., Ulyanov, N.B., Farr-Jones, S., Zhang, H., Donne, D.G., Kaneko, K., Groth, D., Mehlhorn, I., Prusiner, S.B. and Cohen, F.E. 1997. Solution structure of a 142-residue recombinant prion protein corresponding to the infectous fragment of the scrapie isoform. Proc. Natl. Acad. Sci. USA 94: 10086–10091.
35. Donne, D.G., Viles, J.H., Groth, D., Mehlhorn, I., James, T.L., Cohen, F.E., Prusiner, S.B., Wright, P.E. and Dyson, H.J. 1997. Structure of the recombinant full-length hamster prion protein PrP(29–231): The N-terminus is higly flex-

ible. Proc. Natl. Acad. Sci. USA 94: 13452–13457.

36. Harper, E.T. and Rose, G.D. 1993. Helix stop signals in protein and peptides: the capping box. Biochemistry 32: 7605–7609.
37. Holm, L. and Sander, C. 1993. Protein structure comparison by alignment of distance matrices. J. Mol. Biol. 233: 123–138.
38. Arents, G.A. and Love, W.E. 1989. *Glycera dibranchiata* hemoglobin. Structure and refinement at 1.5 Å resolution. J. Mol. Biol. 210: 149–161.
39. Cohen, F.E., Pan, K., Huang, Y., Baldwin, M., Fletterick, R.J. and Prusiner, S.B. 1994. Structural clues to prion replication. Science 264: 530–531.
40. Harrison, P.M., Bamborough, P., Daggett, V., Prusiner, S.B. and Cohen, F.E. 1997. The prion folding problem. Curr. Opin. Struct. Biol. 7: 53–59.
41. Frisch, C., Kolmar, H., Schmidt, A., Kleemann, G., Reinhardt, A., Pohl, E. Us˜òn, I., Schneider, T.R. and Fritz, H.-J. 1996. Contribution of the intramolecular disulfide bridge to the folding stability of REIv, the variable domain of human immunoglobulin κ light chain. Folding & Design 1: 431–440.
42. Lehmann, S. and Harris, D.A. 1996. Mutant and infectious prion proteins display common biochemical properties in cultured cells. J. Biol. Chem. 271: 1633–1637.
43. Daude, N., Lehmann, S. and Harris, D.A. 1997. Identification of intermediate steps in the conversion of a mutant prion protein to a scrapie-like form in cultured cells. J. Biol. Chem. 272: 11604–11612.
44. Lehmann, S. and Harris, D.A. 1997. Blockade of glycosylation promotes acquisition of scrapie-like properties by the prion protein in cultured cells. J. Biol. Chem. 272: 21479–21487.
45. Palmer, M.S., Dryden, A.J., Hughes, J.T. and Collinge, J., 1991. Homozygous prion protein genotype predisposes to sporadic Creutzfeldt-Jakob disease. Nature 352:340–342.
46. Goldfarb, L.G., Petersen, R.B., Tabaton, M., Brown, P., LeBlanc, A.C., Montagna, P., Cortelli, P., Julien, J., Vital., C., Pendelbury, W.W., Haltia, M., Wills, P.R., Hauw, J.R., McKeever, P.E., Monari, L., Schrank, B., Swergold, G.D., Autilio-Gambetti, L., Gajdusek, D.C., Lugaresi, E. and Gambetti, P. 1992. Fatal familial insomnia and familial Creutzfeldt-Jakob disease: Disease phenotype determined by a DNA polymorphism. Science 258: 806–808.
47. Prusiner, S.B. 1996. Molecular biology and pathogenesis of prion diseases. Trends Biochem. Sci. 21: 482–487.
48. Telling, G.C., Scott, M., Mastrianni, J., Gabizon, R., Torchia, M., Cohen, F.E., DeArmond, S.J. and Prusiner, S.B. 1995. Prion propagation in mice expressing human and chimeric PrP transgenes implicates the interaction of cellular PrP with another protein. Cell 83:79–90.
49. Kaneko, K., Zulianello, L., Scott, M., Cooper, C.M., Wallace, A.C., James, T.L., Cohen, F.E. and Prusiner, S.B. 1997. Evidence for protein X binding to a discontinuous epitope on the cellular prion protein during scrapie prion propa-

gation. Proc. Natl. Acad. Sci. USA 94: 10069–10074.

50. Priola, S.A. and Chesebro, B. 1995. A single hamster PrP amino acid blocks conversion to protease-resistant PrP in scrapie-infected mouse neuroblastoma cells. J. Virol. 69: 7754–7758.
51. Koradi, R., Billeter, M. and Wüthrich, K. 1996. MOLMOL: A program for display and analysis of macromolecular structures. J. Mol. Graph. 14: 51–55.
52. Hochuli, E., Döbeli, M. and Schader, A. 1987. New metal chelate absorbent selective for proteins and peptides containingneighbouring histidine residues. J. Chromatogr. 411: 177-184.